Arab J Geosci (2013) 6:4257–4269
DOI 10.1007/s12517-012-0684-5

ORIGINAL PAPER

Recent analog of gypsified microbial laminites and stromatolites in solar salt works and the Miocene gypsum deposits of Saudi Arabia and Egypt

Mahmoud A. M. Aref · Rushdi J. A. Taj

Received: 17 January 2012 / Accepted: 4 September 2012 / Published online: 18 September 2012

Abstract Accumulation of microbial mats and stromatolites dominate in the crystallization ponds of solar salt works west of Alexandria, Egypt. These microbial mats are laminar in the permanent submerged part of the ponds. The microbial mats commonly form sites for growth of gypsum crystals during periods having higher salinity. In the dominant submerged part of the pond, domal stromatolites are common around groundwater seepage holes. In the shallow, intermittent margin of the ponds, the laminated microbial structure forms laterally close-linked hemispheroidal stromatolite type, with unidirectional and multidirectional ripple mark-like morphology on their surface. The microbial laminite and stromatolite types in the modern solar salt works are similar to the organic-rich Miocene gypsum beds of El-Barqan (west Alexandria, Egypt) and Rabigh (north Jeddah, Saudi Arabia). The Miocene organic-rich beds consist of interlayered dark-colored microbial laminae and light-colored gypsum laminae. These beds may have three different variations: regular even lamination, laterally closed-linked hemispheroidal stromatolites, and/or discrete hemispheroidal stromatolites. Petrographic examination of the microbial laminites and stromatolites in the solar salt works and the Miocene gypsum beds indicate that the dark-colored, organic-rich laminae are composed of micritized microbial laminae and/or brown organic filaments. In El-Barqan area, the light-colored gypsum-rich laminae are composed of either gypsum crystal fragments, or lenticular and prismatic gypsum. These gypsum crystals are either entrapped within the microbial filaments or are nucleated at the surface of the microbial laminae to form a radial pattern, whereas in Rabigh area, the light-colored gypsum-rich laminae are composed of secondary porphyrotopic, poikilotopic, or granular gypsum crystals. By comparison of the microbial structure in the Miocene gypsum beds with the recent occurrence of the microbial laminites and stromatolites in the solar salt works, it is demonstrated that the organic-rich Miocene gypsum beds were formed in a very shallow salina with slightly fluctuating brine levels.

Keywords Microbial laminites · Stromatolites · Gypsum · Salt works · Miocene · Saudi Arabia · Egypt

M. A. M. Aref (✉) · R. J. A. Taj
Department of Petroleum Geology and Sedimentology, Faculty of Earth Sciences, King Abdul Aziz University, Jeddah, Saudi Arabia
e-mail: m1aref@yahoo.com

R. J. A. Taj
e-mail: rtaj@kau.edu.sa

Present Address:
M. A. M. Aref
Geology Department, Faculty of Science, Cairo University, Giza, Egypt

Introduction

Environments of hypersaline deposition have received increased attention in recent years because of the increased recognition that hypersaline sedimentation might be a potential source for oil (Russell et al. 1997; Schreiber et al. 2001), the association of several heavy metals in both evaporites and their stromatolitic association (Gerdes and Krumbein 1987; Taher et al. 1995; Scheiber 2004; Scheiber et al. 2007; Kato et al. 2009), and the influence of microbial processes on the quality of commercial salt production (Davis and Giordano 1996; Magaña et al. 2005; Davis 2009). In addition, much of our knowledge concerning ancient sedimentary facies of evaporites and siliciclastics and their depositional environments has been derived from the study of modern sedimentary environments, for example tidal flats (Noffke et al. 1996 and 2007; Eriksson et al. 2007; Gerdes 2007; Cuadrado et al.

2011) evaporitic sabkhas (Duane and Al-Zamel 1999; Stivaletta et al. 2006; Basyoni and Aref 2007; 2011; Taj and Aref 2009, 2011), salinas (Cornee et al. 1992; Aref 2000; Oren et al. 2009), and under subtidal conditions (Dill et al. 1986; Glunk et al. 2011). Modern models for stromatolite formation in evaporitic environments are those based on the sabkhas of the Arabian Gulf (Kendall and Skipwith 1968), hypersaline lagoons and lakes (Cohen et al. 1984; Jones and Hunter 1991), and large tide-free salt works (Orti Cabo et al. 1986; Cornee et al. 1992). Further information on microbialites has been obtained from Quaternary coral reefs (Webb et al. 1998; Cabioch et al. 2006). Modern stromatolites that form in such environments range in size from giant subtidal types growing in normal salinity waters of the Bahamas bank (Dill et al. 1986) to centimeter-sized examples in the Arabian Gulf (Kendall and Skipwith 1968; Duane and Al-Zamel 1999).

Hypersaline environments in which microbial growth flourish (stromatolites and laminites) have been described for the Holocene gypsum deposits of Ras El-Shetan (Aref 1998), the Miocene gypsum deposits of El-Barqan area, north Western Desert of Egypt and Rabigh area, Red Sea, Saudi Arabia (Aref 2003). Comparison of recent microbial mat systems in Borg El-Arab solar salt works (Fig. 1), with the assumed ancient analog in the Miocene evaporites of Egypt and Saudi Arabia, may help to understand the environmental conditions necessary for the variable morphologies of stromatolites, similar to those interpreted by Knoll (1985), Krumbein (1985), and Stivaletta et al. (2006).

Nomenclature

In this work, the nongenetic definition of stromatolites recommended by Semikhatov et al. (1979) and Pope et al. (2000) is given as: "an attached, laminated, lithified sedimentary growth structure, accretionary away from a point or limited surface of initiation." This definition is particularly considered by Pope et al. (2000) as it provides a concise statement of the basic geometric and textural properties of all stromatolites while at the same time allowing for multiple or even intermediate origins.

When microorganisms of cyanobacteria cover sedimentary grains, it forms adhesive organic envelopes. Such organic coatings are termed biofilms (Costerton and Stoodley 2003). At sites of favorable ecological conditions, biofilms continue to grow to form thick and significant organic layers termed microbial mats (Krumbein 1983). The term "microbial mat" is preferentially used by Gerdes and Krumbein (1987), Gerdes (2007), and references therein to denote modern analogs of stromatolites in the unconsolidated state. Microbial mats of varying composition are also termed "potential stromatolites" (Krumbein 1983).

Study areas

Borg El-Arab solar salt works

Physiography and hydrology

West of Alexandria, the coastal plain of Egypt consists of a series of eight linear ridges that run more or less parallel to the coast. The three ridges nearest to the Mediterranean Sea are continuous for long distances, and separate depressions filled with colluvium and sabkhas (Aref 2000). The Borg El-Arab solar salt works (10 km long×4 km wide) are situated in the second depression (Mallahet Maryut Depression). Seawater (3–5 Baumé) is pumped from the Mediterranean Sea and enters the infiltration ponds. The water runs through a series of large concentration ponds and finally into crystallization ponds where halite precipitates (22.0 Baumé). A significant contribution of groundwater seepage from El-Nasr canal to the crystallization ponds reduces the brine salinity to 10 Baumé and favors the development of potential stromatolites and microbial laminites in the halite crystallization ponds.

Climate

The southern coast of the Mediterranean Sea has a semiarid climate. Temperature ranges from 13.6 to 29 °C. Rainfall is absent during summer months (May–September), and the maximum rainfall is 24.9 mm in January. Monthly evaporation rate ranges from 9 to 19.6 mm. Wind is mostly from the northwesterly direction. The humidity ranges from 60 to 82.2 %. The climatic data denote dry, hot summer months, which favor precipitation of evaporite minerals, and the relatively wet winter months, coupled with much contribution of groundwater seepage, favor flourishing of microbial activity, but not a complete return to open marine conditions.

Sedimentology

The western and southern margins of the halite crystallization ponds have numerous seepage points and inflow of groundwater, which markedly decreases the salinity from 22 Baumé to less than 10 Baumé. At these locations, microbial activities are widespread that can form stromatolites and microbial laminites.

Stromatolites develop in the mat-covered sediments of the dominantly submerged parts of the solar ponds to a depth of 70 cm. They commonly surround or are adjacent to a groundwater seepage hole (depth >2 m; Fig. 2a). According to the brine depth, stromatolites form three patterns that differ in size and arrangement. The first is recorded at the deeper part of the pond as large stromatolites

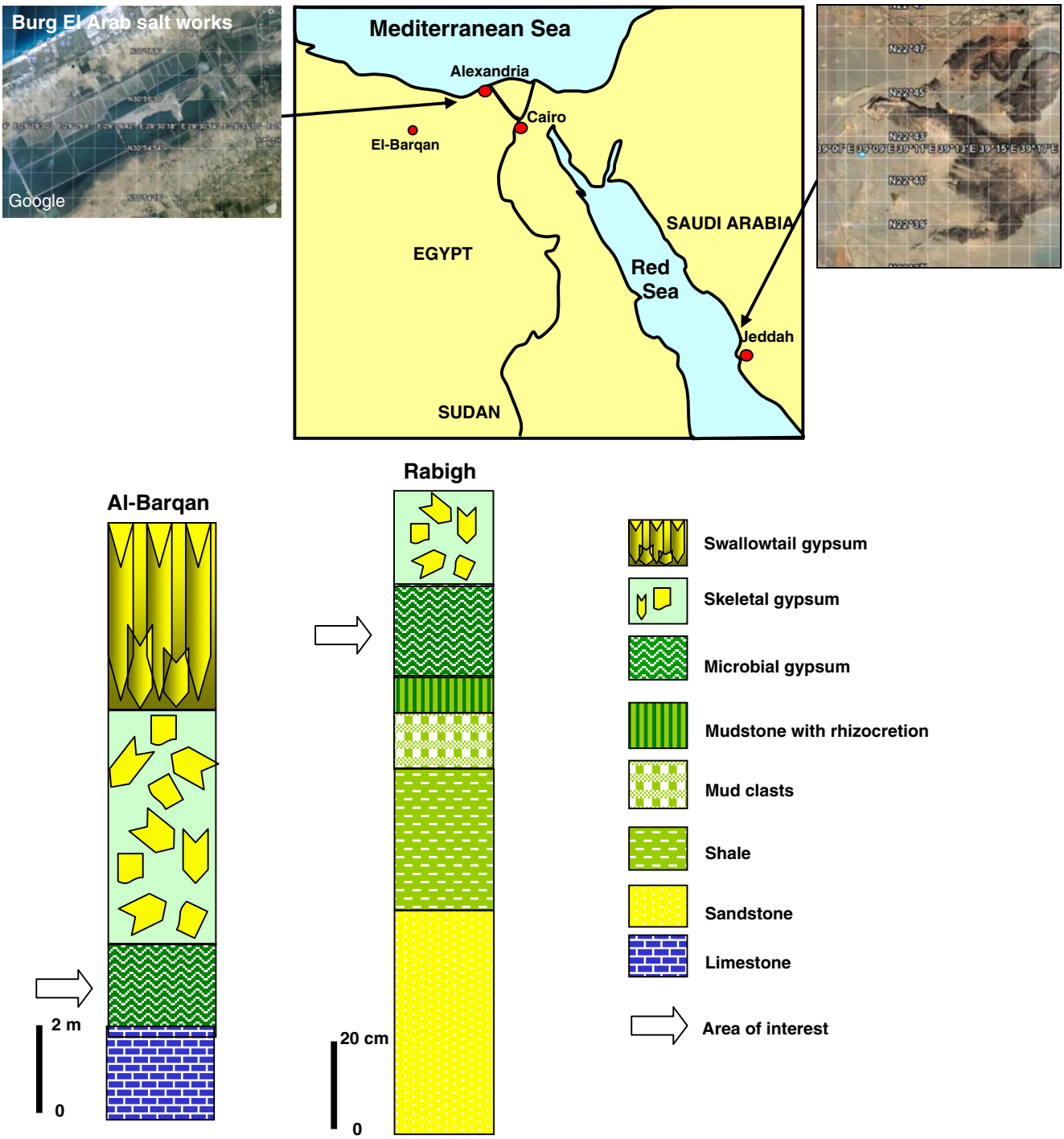

Fig. 1 Location map and lithologic logs of the study areas in Saudi Arabia and Egypt

with a height of 30 cm and width of 50 cm. They form individual domal structures that protrude from the water surface (Fig. 2b). The second is recorded at the shallower part of the pond (~20 cm depth) as smaller domal stromatolites with a height of <15 cm and width of 20 cm. They form numerous individual or merged domal structures (Fig. 2c). The third type is recorded near the margin of the pond (<10 cm brine depth). In this type, stromatolite domes form island-like patches that are surrounded with the brine (Fig. 2d). Generally, the stromatolites may be composed of a single dome or several smaller (<5 cm) domal structures that have a common basal attachment to the substrate. In the area of dominant domal stromatolites, the submerged part of the pond forms a rippled surface that appears to be composed of

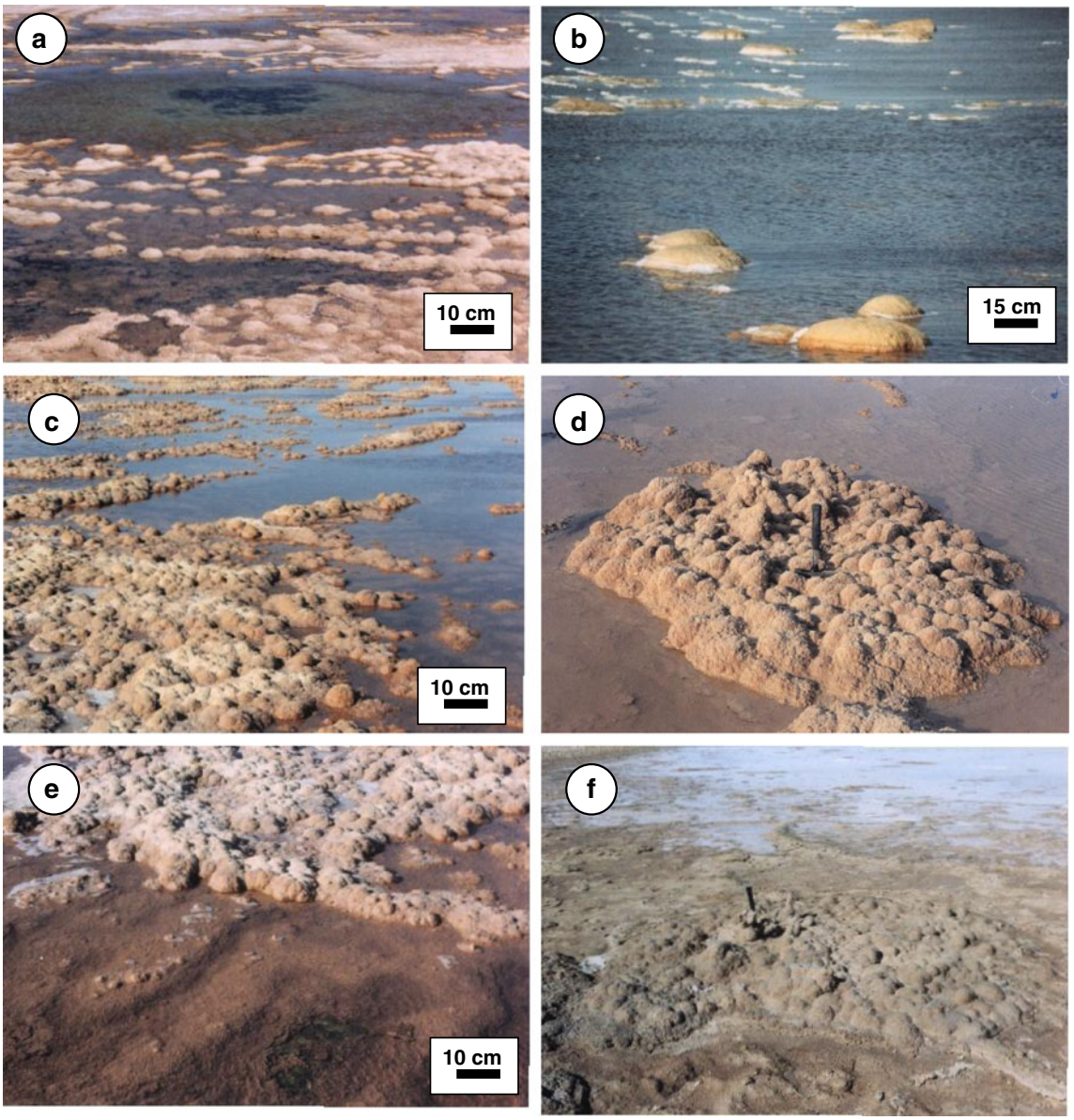

Fig. 2 Domal stromatolites at different depths of the saline ponds. **a** Gypsified stromatolite domes growing around a seepage groundwater hole (2 m in depth). **b** Large, individual domal stromatolites in the deeper part (>50 cm) of the pond. **c** Small, numerous, individual domal stromatolites partially exposed in the shallow brine pond. **d** A table-like patch composed of aggregates of domal stromatolites. **e** Partially exposed domal stromatolites adjacent to submerged rippled microbial mats. Notice the small domal stromatolites growing on the crest of the ripples. **f** Numerous domal stromatolites exposed due to desiccation and withdrawal of the brine

yellow- and brown-colored cyanobacteria, underlain with green cyanobacterial mats (Fig. 2e), similar to that described by Gerdes et al. (1984) and Oren et al. (1995, 2009). On the crest of the rippled surface, small (<3 cm in dimension) domal stromatolites grow and have a preferred orientation (Fig. 2e).

During summer months (July–September), withdrawal of the residual brine in order to harvest halite leads to drying of the pond and emergence of the stromatolite heads. It is found that at the interior part of the ponds, the second type of the domal stromatolites covers the entire floor of the desiccated ponds. They have slightly variable sizes, which may be controlled by the ground topography. At the margin of the ponds, the third type of the stromatolite domes forms 3–7 m in width patches that exist at slightly higher elevated levels where the surrounding, less elevated ground is barren of stromatolite heads (Fig. 2f).

Examination of the vertical section of the domal stromatolites revealed that they are composed of raised arched, gypsified, microbial layers over a central cavity (Fig. 3a, b). The cavity is filled with gas that originates from decaying subrecent mat materials in deeper parts of the sediment. Ongoing

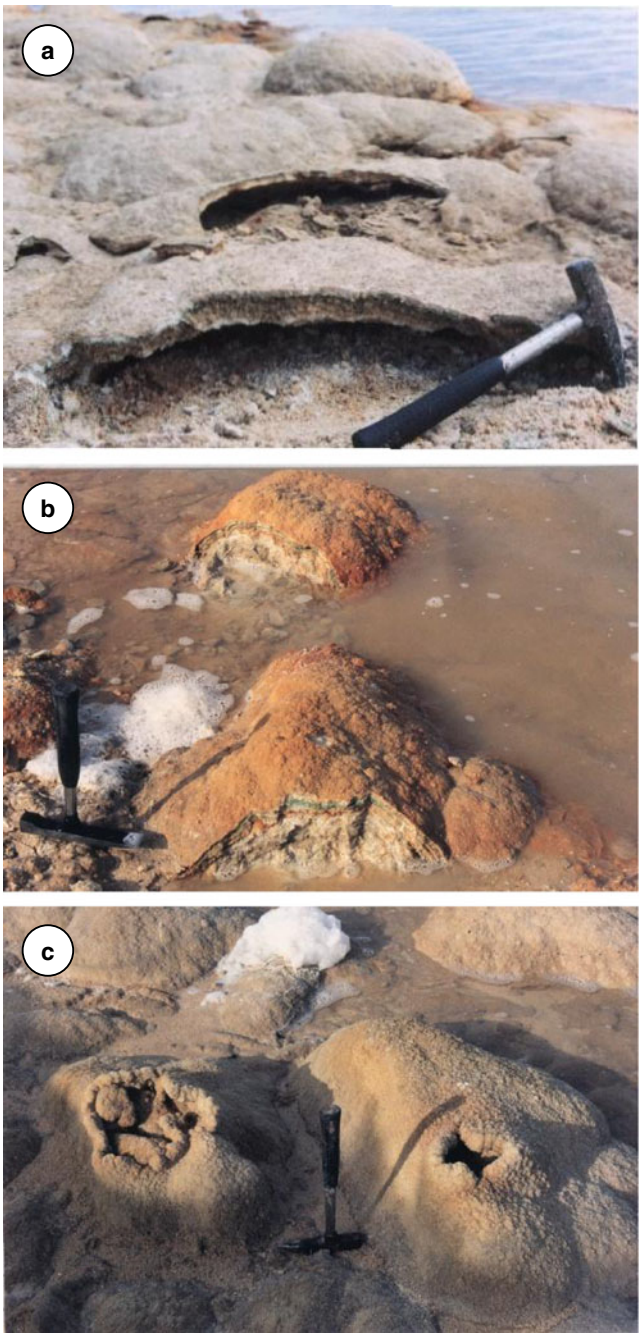

Fig. 3 Gypsified stromatolite domes. **a** A vertical section in the domal stromatolites shows a thin upheaval crust of gypsum and microbial laminae over a central cavity. **b** A vertical section in the domal stromatolites shows a thick upheaval crust composed of gypsum and multicolored microbial laminae. **c** An opening on the crest of the domal stromatolites encrusted, together with the dome, with gypsum crystals

accumulation of gas beneath the surficial mat increases gas pressure so that domes are formed locally (Noffke et al. 1996).

The domal stromatolites are composed of centimeter-thick layers composed of alternations of white and colored laminations. The colored laminae are represented by green cyanobacterial mat near the top, brown, and red sulfate-reducing bacteria near the bottom (Fig. 3b). The white laminae are composed of stacked vertically growing rosette of gypsum crystals that encrust the microbial laminae. The surface of the stromatolite heads may be closed (Fig. 2b–d) or have circular opening connected to the central cavity (Fig. 3c).

At the very shallow intermittent part of the ponds (<10 cm in depth), as well as at their margins, microbial mats form elongated, straight, and/or twisted crinkled surfaces that exhibit ripple-mark morphology (Fig. 4a, b). The ripple marks have generally NE–SW orientation in the submerged part of the pond, as well as in most parts of the desiccated margin of the pond, which is normal to the general northwesterly wind direction. In the latter setting, the ripple marks may take different orientation, where the microbial mats dried up and form twisted or straight arched crust (Fig. 4c). The latter structure is very similar to the multidirected ripple mark structure described in clastic sediments by Noffke et al. (1996, 2001), Noffke (1998), Draganits and Noffke (2004), Beukes and Lowe (2006), and Scheiber et al. (2007). Close examination of these crinkled microbial mats indicates that they consist of flat, finely laminated wrinkled to wavy discontinuous laminae that form laterally close-linked hemispheroid (type LLH-C of Logan et al. 1964) (Fig. 4d). The hemispheroids are composed of ~5-cm-thick domed crust over hollow central cavity. These crusts are composed also of multicolored microbial laminae and light-colored gypsum laminae. The microbial laminae, similar to the domal stromatolites, are composed of green cyanobacterial laminae at the top and brown to red sulfate-reducing bacterial laminae at the bottom. The white laminae are composed of rosette gypsum crystals that encrust the microbial laminae.

The dominantly emerged part of the ground, close to the solar pond, is either covered with a very thin water film or wet due to the close proximity to the water table. In this wet saline zone, the surface is covered with colorful zonation of yellow and green cyanobacterial filaments (Fig. 5a), red layer of phototrophic sulfur bacteria, and at depth a black zone of sapropelic appearance which is formed by anaerobic sulfate-reducing bacteria, similar to description by Gerdes et al. (1984), Taher et al. (1995), and Oren et al. (2009). Growth of gypsum in this zone is dominant through the displacive growth of lenticular crystals within microbial filaments that lead to the development of highly twisted protuberances, known as petee structures (Fig. 5b).

Microscopic examination of the domal stromatolites (discrete hemispheroids), and the crinkled microbial mats (laterally close-linked hemispheroid), revealed that the light-colored laminae are composed of vertically oriented gypsum crystals in prismatic to rosette clusters (>2 mm in length) that nucleated over the microbial laminae. The colored microbial laminae are composed of either a dense microbial carbonate micrite or microbial filaments that trap and bind

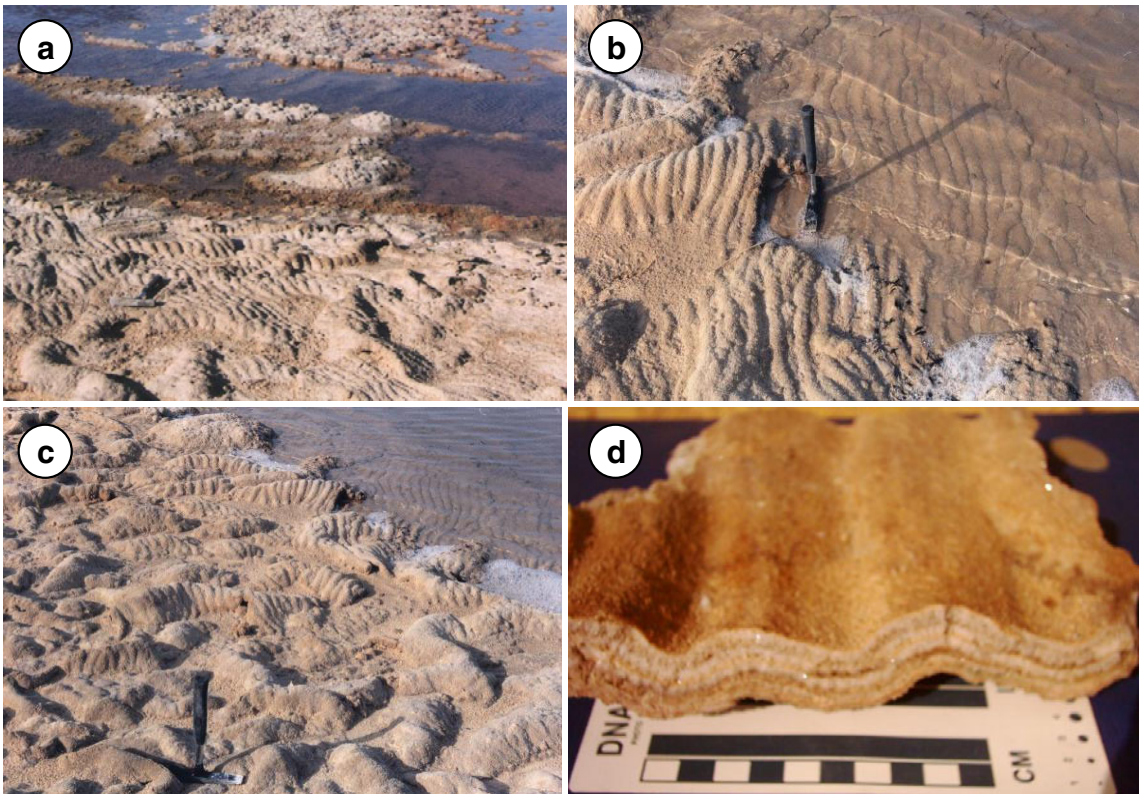

Fig. 4 Crinkled gypsified microbial mats. **a** Growth of the domal stromatolites at the deeper part of the pond, whereas the rippled microbial surface grew at the shallow agitated part of the pond. **b** Crinkled microbial mats that show unidirectional ripple marks on their surfaces. **c** Buckling of the crinkled, rippled microbial mats into elongated domes with variable orientations that show multidirection of the ripple marks on their surfaces. **d** Close-up of the crinkled gypsified microbial mats showing a rippled surface and laterally close-linked hemispheroids

the gypsum crystals. On the other hand, the emerged petee structures (the dominant form) are composed of dense microbial micrite with displacive growth of lenticular or prismatic gypsum crystals (Fig. 5c). These laminations are commonly covered with reworked clastic gypsum.

El-Barqan Miocene evaporites

El-Barqan area is located in the north Western Desert of Egypt at 50 km south of the present-day Mediterranean coast, and 60 km southwest of Borg El-Arab solar salt works (Fig. 1). Quarrying of gypsum in El-Barqan area revealed relatively thin Miocene evaporites when compared with other Mediterranean evaporites (Aref 2003). The outcropping gypsum sequence (3–8 m thick) is represented by three beds (Fig. 1); the lower is microbial (laminoids and stromatolitic) gypsum, the middle is skeletal and grass-like gypsum, and the top is composed of coarse, vertically oriented twinned selenite. The attention is given here to the lower microbial gypsum bed.

The lower microbial gypsum bed represents the transitional stage from the normal marine carbonate of the Middle Miocene Marmarica Formation to the Messinian sulfate evaporites (Aref 2003). The microbial gypsum layer varies in thickness from 100 to 180 cm, depending on the degree of exposure of the base. The microbial gypsum bed displays laminations and textures that can be subdivided into three horizons: lower, middle, and upper. The lower horizon is composed of flat to slightly wavy continuous microbial laminae (Fig. 6a), 20–30 cm thick, and consists of thin, dark-colored microbial laminae (1–2 mm thick) and thicker white gypsum laminae (5–9 mm). This horizon is overlain by a middle horizon that consists of slightly to highly wavy thin dark microbial laminae and thicker white gypsum laminae (63 cm thick), similar to the lower horizon, but with a greater degree of contortion and discontinuity of the microbial laminae (Fig. 6a). The laminations consist of hemispheroids, with a height less than 3 cm and width of 7 cm, with rounded crests and troughs. The hemispheroids are laterally linked forming laterally close-linked hemispheroid type of Logan et al. (1964). Surface exposure of the middle horizon shows a ripple mark morphology, composed of elongated, bifurcated ridges, and intervening rounded troughs (Fig. 6b). The upper 20 cm of this horizon shows slight deformation and doming of the microbial laminae by displacive growth of vertically oriented gypsum crystals (Fig. 6a).

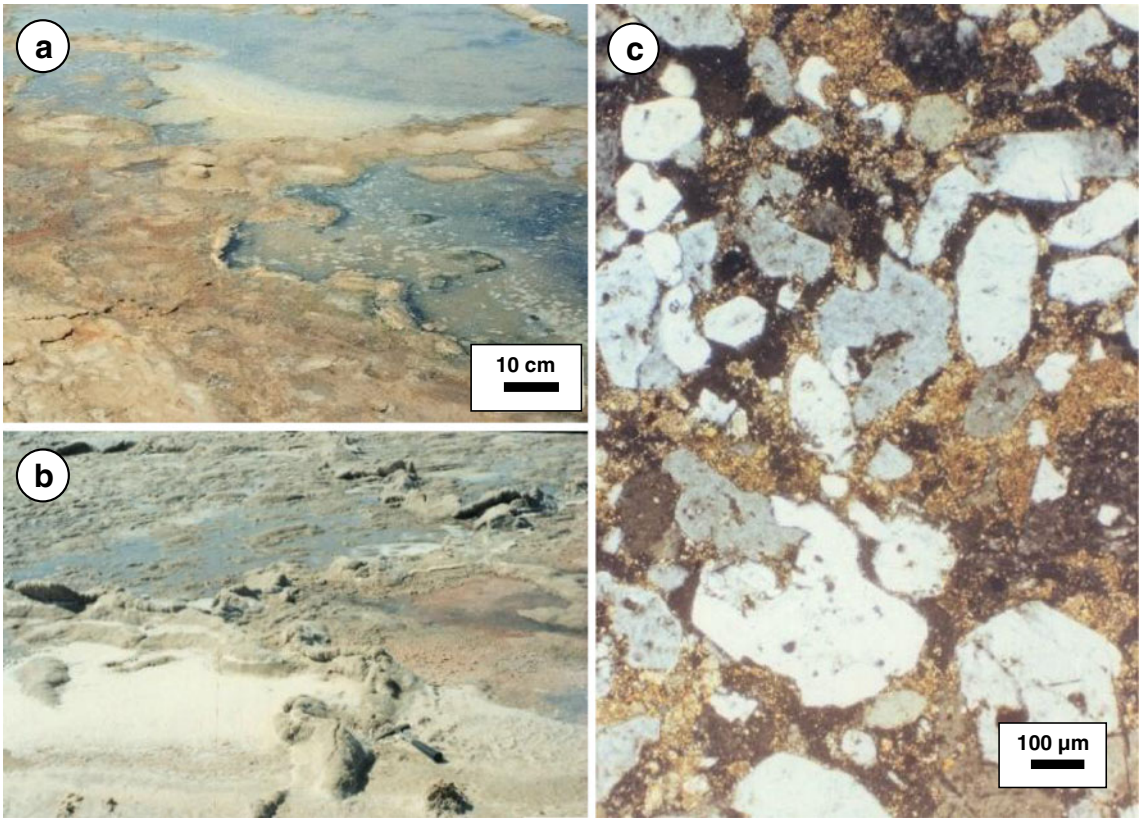

Fig. 5 Surface structure of the sabkha. **a** A versicolored surface of the brine due to various population of cyanobacteria and diatoms. **b** Buckling of the desiccated sediment surface into protuberance petee structure due to the interplay of biogenic and physical processes. **c** Prismatic and clastic gypsum entrapped within microbial micrite, Polars Crossed

The upper horizon, 30–60 cm thick, loses continuity in lamination of the microbial layer due to sporadic growth of numerous gypsum crystals 3 cm in length (Fig. 6c). The growth of gypsum below the delicate microbial laminae forms discrete, individual domal stromatolite, centimeters in height. Surface exposure of this horizon shows miniature

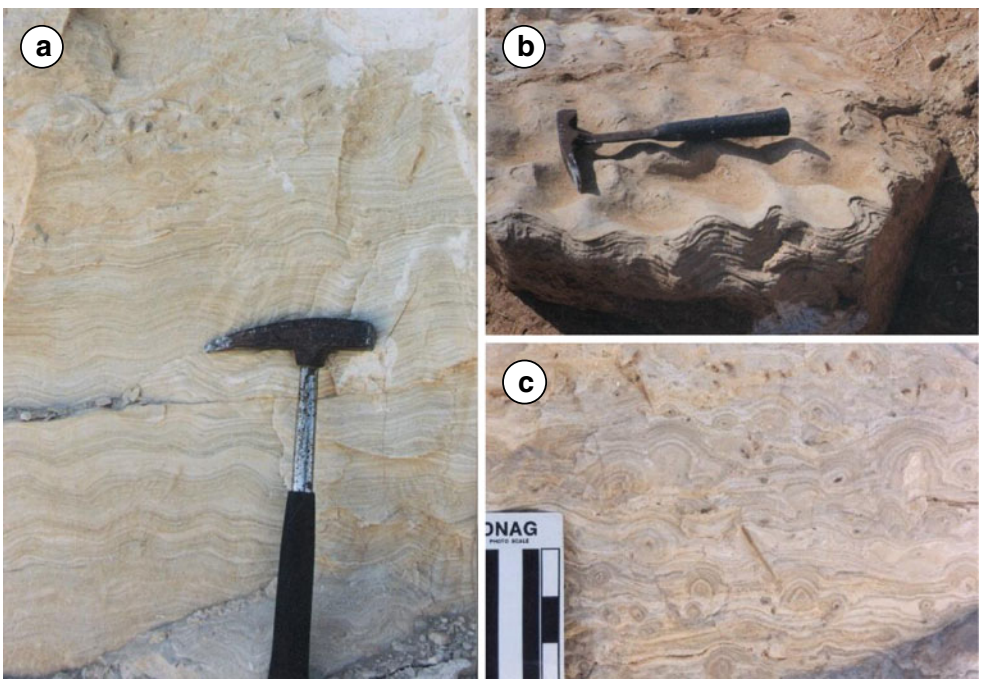

Fig. 6 Microbial laminites in the Miocene gypsum of Egypt. **a** Interlamination of dark-colored microbial laminae and light-colored gypsum laminae that show a flat lamination at bottom, wavy lamination at middle, and distortion of lamination at top due to growth of prismatic gypsum. **b** Surface exposure of the wavy lamination in Fig. 6a shows ripple marks on the surface. **c** Discontinuities of the microbial and gypsum laminae due to the displacive growth of gypsum crystals

small, smooth individual domes, with up to 3 cm of relief between the tops of the domes and their intervening troughs (Fig. 7a). This morphology is closely similar to type discrete stacked hemispheroids (type SH-V) of Logan et al. (1964). The microbial laminae are thin at the crest of the hemispheroids and thicker at their flanks and in spaces between adjacent hemispheroids.

Microscopic examination of the microbial gypsum bed revealed repeated white gypsum and dark microbial units a few millimeters thick (Fig. 7b). Upwards, from base to top of the white gypsum laminae, gypsum crystals (250–600 μm) are anhedral, with straight boundaries and an equant grain size (gypsarenite of Warren 1982) that grade upwards into fine (40–80 μm) gypsum crystals. This normal grading laminae range in thickness from 2.5 to 8 mm. Superimposed on this gypsum laminae is an upper organic-dominated laminae built by calcitized microbial mats (Fig. 7b). The organic laminae are represented by a condensed meshwork of micritized microbial filaments (1–2 mm thick) that bind and trap 20–40-μm gypsum crystals.

The upper horizon of the microbial gypsum bed shows that the characteristic normal grading of the lower and middle horizons is disturbed due to displacive growth of upright selenitic gypsum crystals (Aref 2003). The displacive selenite crystals are usually surrounded with a thicker zone of clear, coarse gypsum and a thinner zone of micritized microbial filaments rich in fine gypsum. Deformation of the irregular lamination suggests displacive growth of the selenitic gypsum. Some of the microbial laminae in the upper horizon contain fenestral structures surrounded with gypsum (Fig. 7c), which form by trapping and binding of gypsum crystals by microbial filaments.

Rabigh Miocene evaporites

Rabigh area is located north of Jeddah city by 170 km at the Red Sea coast of Saudi Arabia (Fig. 1). Taj and Hegab (2005) studied the lithostratigraphy, sediment characteristics, and depositional environments of the Miocene Dafin Formation of Moore and Al-Rehaili (1989) in Rabigh area, and they classified Dafin Formation into three sedimentary lithologies: siliciclastic, carbonate, and evaporite rocks. The siliciclastic sediments are widely exposed in most of the eastern part of Rabigh area at Wadi Al Haqqaq, Wadi Al Hajar, and Wadi Al Jarba. The carbonate deposits are exposed at the south eastern part of the sedimentary cover (at

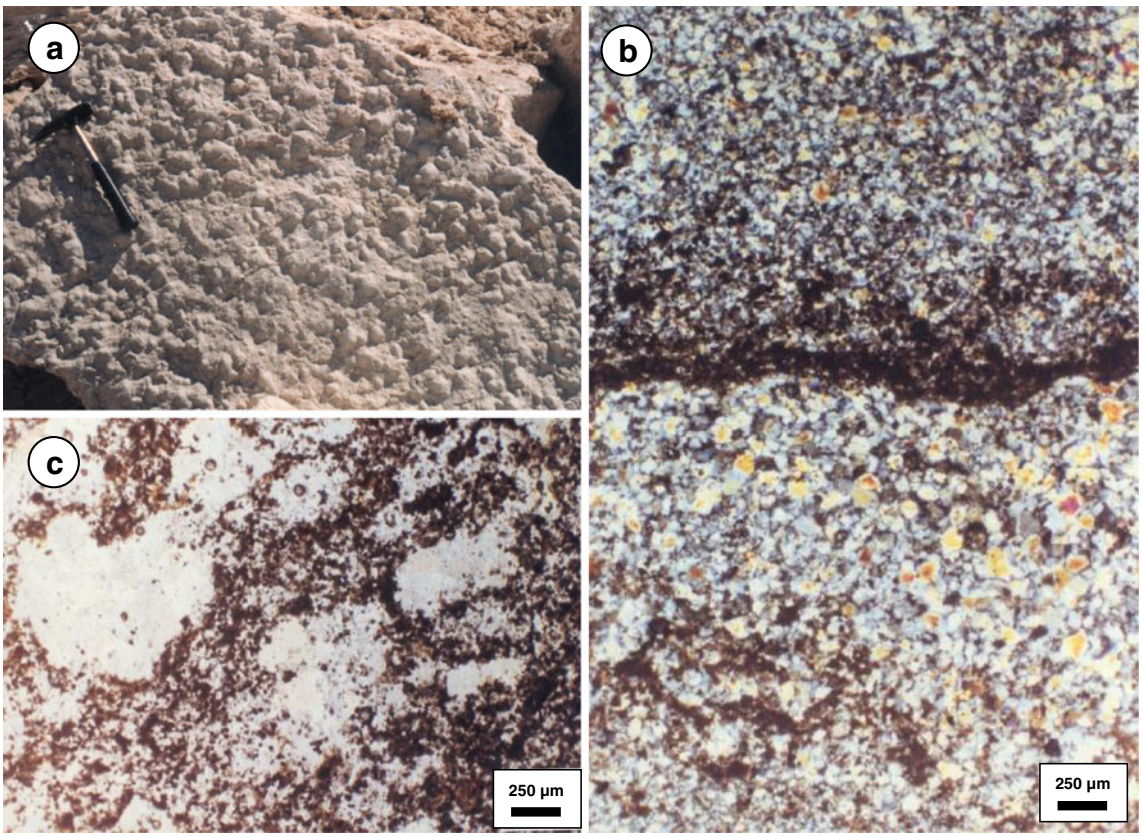

Fig. 7 **a** Surface exposure of Fig. 6c shows individual domal stromatolites with synoptic relief. **b**, **c** Photomicrograph of the gypsum and microbial laminations. **b** Clear zone composed of gypsarenite, overlain with dark zone composed of microbial filaments and entrapped gypsum crystals, Polars crossed. **c** Dark-colored microbial micrite entraps and binds clear gypsum crystals, Plane light

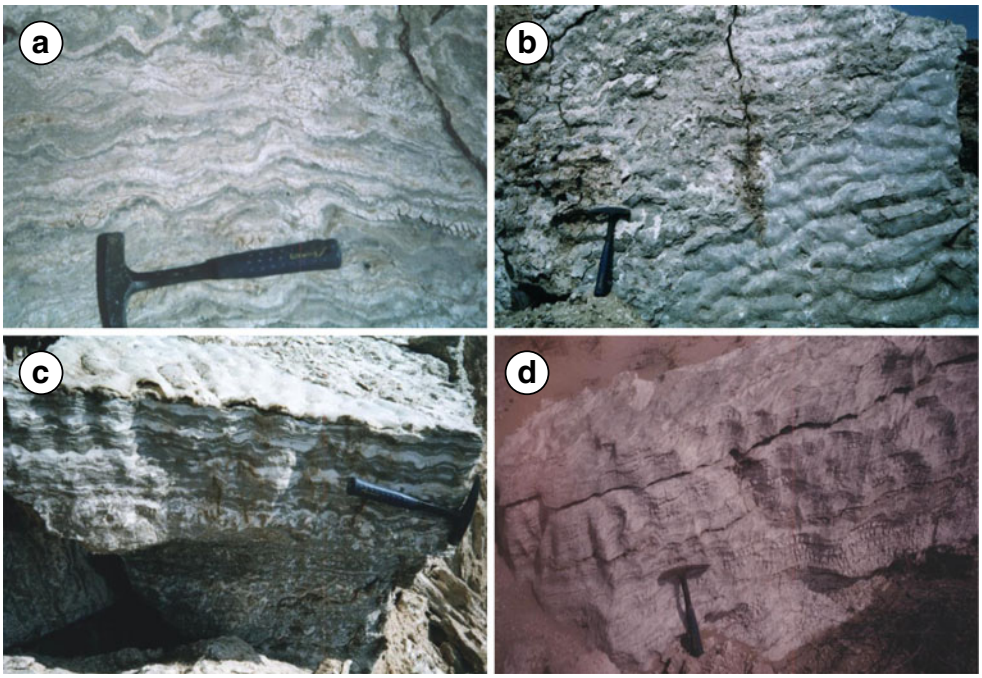

Fig. 8 Interlamination of microbial laminae and gypsum laminae. **a** Interlamination of dark microbial laminae and lighter gypsum laminae that form wavy lamination. **b** Surface exposure of the wavy lamination shows elongated ripple marks. **c** Contact between the wavy lamination and the massive layer that resulted from displacive growth of gypsum crystals (gypsum block is upside down). **d** Slightly irregular interlamination of microbial laminae and gypsum laminae

Wadi Al Jarba) and consist of unfossiliferous limestone, foraminiferal limestone, and coralline limestone (Mandurah and Aref 2011; Taj 2012). The third lithology, the evaporites, is exposed at the most northwestern part of the sedimentary cover (at Miqat Al Jahfah). The evaporite sequence conformably overlies the siliciclastics and increases in thickness towards north and northwest.

At outcrop and in active gypsum quarries, the evaporite sequence is composed of secondary gypsum with a dominance of microbial-laminated and stromatolitic structures (Mandurah and Aref 2010; Aref and Mandurah 2011). At the southern side of the evaporite exposure, the outcropping evaporite sequence consists of three somewhat different facies (from base to top): 50-cm-thick white gypsified stromatolitic layer, 15–20-cm-thick massive gypsum, and 120-cm-thick microbial-laminated gypsum. At the quarries, the evaporite sequence is composed of several gypsum layers that are interbedded with mudstone and sandstone layers. The gypsum layers are composed dominantly of irregular and regular microbial-laminated structures, similar to those described in outcrop.

The lower stromatolitic gypsum layer is composed of wavy microbial laminae that form laterally linkage stromatolite heads. The stromatolite layer is formed by a thick (3–5 cm) gypsum bed that is interlayered with thinner (<1 cm) greenish to brownish carbonate laminae (Fig. 8a). On the bedding surface, the stromatolitic gypsum forms a ripple-like morphology of irregular, non-bifurcated or bifurcated crests (Fig. 8b).

The middle massive gypsum layer is composed of slightly reworked, white gypsum crystals (<3 cm long) that are dispersed in greenish carbonate mud (Fig. 8c). The upper

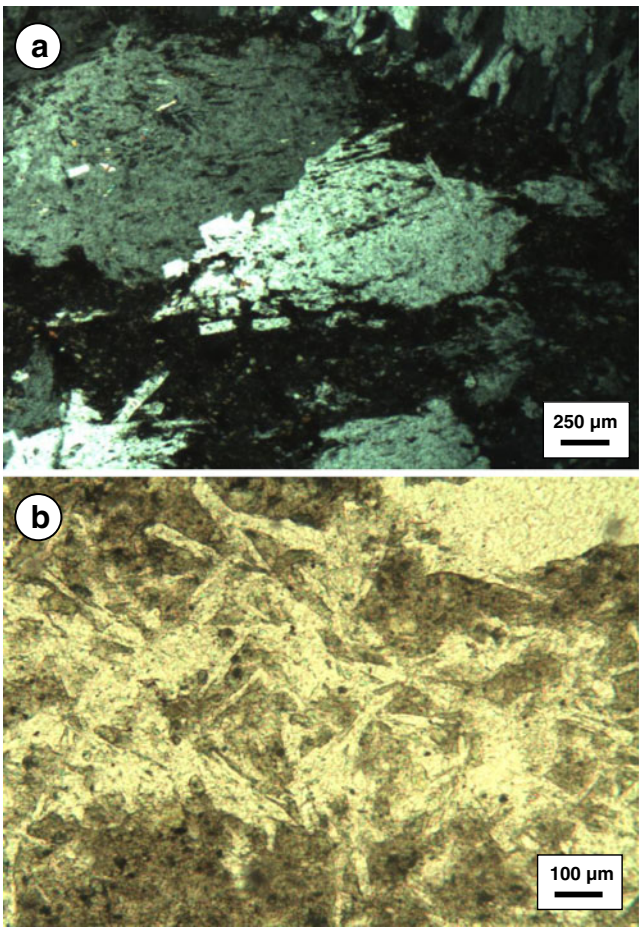

Fig. 9 Photomicrograph of the gypsum laminae. **a** Dark irregular laminae composed of dense micrite with coarse porphyrotopic gypsum crystals intersect the laminations (Polars crossed). **b** Ghost of prismatic gypsum crystals in between the microbial micrite (Plane light)

laminated gypsum layer is formed of slightly irregular thin, dark green to brown microbial carbonate laminae and thicker white to pale grey or yellow gypsum laminae (Fig. 8d). The last facies has a significant thickness and forms the greater portion of the quarries.

Microscopic examination of the stromatolitic and microbial gypsum beds revealed both repeated dark microbial laminae and white gypsum laminae. The microbial micrite is composed of dense micrite grains, sporadically with black organic matter that is aggregated to form dense laminae (Fig. 9a). The laminae may be continuous for a long distance or broken into short parallel laminae. The microbial micrite laminae are relatively thin (<200 μm), in contrast to the thicker (>500 μm) gypsum laminae that are composed of porphyrotopic, poikilotopic, and granular gypsum (Fig. 9a). The growth of the porphyrotopic, poikilotopic, and granular gypsum usually intersects and encloses several areas of the earlier gypsum-microbial micrite lamination.

The microbial micrite may preserve the morphology of lenticular and prismatic gypsum crystals within the thick micrite lamination (Fig. 9b) or entrap and bind gypsum crystals by free-floating microbial filaments.

Discussion and conclusions

The structural diversity of both the modern and Miocene microbial (stromatolites and laminoids) deposits is controlled by two dominant factors, namely by depositional dynamics and by the activity of phototrophic microorganisms (like cyanobacteria, bacteria, and diatoms) that colonized the sediments (Noffke et al. 1996; Gerdes 2007). The structures produced by microbial processes such as biostabilization, gas production, and the interplay between sedimentation and microbial growth are well described by Noffke et al. (2001) and Bose and Chafetz (2009) as "Microbially Induced Sedimentary Structures (M.I.S.S.)," which differ from the physical structures of similar appearance (for example ripple marks).

In the solar salt works, similar to the observations and interpretation presented by Noffke et al. 1996), two main types of colonization of the sediments by cyanobacteria can be distinguished: biofilms and microbial mats. In the colored zone, coccoid cyanobacteria are irregularly distributed in the surface layer forming biofilm (Noffke et al. 1996). Filamentous taxa, which are the predominant constructors of microbial mats, can develop at sites where plant cover, grazing animals, deformative burrowing, low sedimentation rate, and physical agitation are excluded. Noffke (1998) found that the coccoid cyanobacteria dominate the microbial assemblages at sites of great hydrodynamic stress, whereas the filamentous cyanobacteria dominate in the areas of lower hydrodynamic stress. When the environmental conditions of the ponds are suitable to the development of microbial mats, the typical varicolored sedimentary surface forms, which represents a multilayered mat system, composed of different bacteria and cyanobacteria (Gerdes et al. 1993; Stivaletta et al. 2006; Oren et al. 2009).

The observed laminations in Borg El-Arab, El-Barqan, and Rabigh areas are most commonly generated by the alternating processes of deposition and microbial growth. The in situ production of biomass at the sedimentary surface corresponds with periods of non-burial or non-erosional conditions (Gerdes et al. 1991), and the non-colonized layers reflect periods of gypsum precipitation. When the sedimentation rate is low, the microorganisms can escape burial by upward migration to the new surface and are reestablished.

Comparison between microbial deposits in the recent solar ponds and the Miocene gypsum

The microbial deposits occurring in Borg El-Arab salt works, as compared to the Miocene gypsum of El-Barqan and Rabigh areas, show many similar features such as: well-developed laminae and abundant occurrence of cyanobacterial mats, occurrence of flat layering and wavy microbial laminoids (Figs. 4d, 6a, and 8a), ripple marks (Figs. 6b and 8b), and stromatolites (Figs. 2f and 7a).

At the same time, there are some differences between the Modern and Miocene microbial gypsum deposits, such as the size and the mode of growth of the discrete hemispheroids stromatolite types (Figs. 2f and 7a), the existence of a residual cavity below the domed stromatolites of Borg El-Arab (Fig. 3a, c), and the upward deformation of the delicate microbial laminae by growth of underlying gypsum crystals (Fig. 6c). The observed difference may be related to different sedimentary environments, where the microbial deposit of El-Barqan most commonly originated in marginal lagoonal environment, and show desiccation and displacive growth of gypsum from groundwater brines, in contrast to the low dynamic environment of the salt works. The dominant microbially laminated structure in Rabigh area indicates the existence of favorable condition for strong microbial activity in a slowly subsiding basin that has a slight variation in salinity during deposition of gypsum or calcitized microbial laminites and stromatolites.

The observed sedimentary structures are not formed exclusively by physical forces, but result from bacterial activity that influences erosional and depositional dynamics. In the solar ponds, the microbes are represented by biofilms and mats. The biofilms do not seem to contribute much to the cohesion of sedimentary grains, whereas mats significantly stabilize the sedimentary surface, which leads to local conservation of earlier physically shaped surface relief at microbially overgrown sites (Noffke 1998). In the solar ponds, the crinkled microbial mats have unidirectional ripple marks at the submerged part of the pond and

multidirectional ripple marks at the desiccated margin of the pond (Fig. 4b and c, respectively). The latter structure is similar in morphology to the oriented ripple marks ("multidirectional ripple marks") of Noffke (1998), but it develops due to a different mechanism wherein ripple marks of similar orientation were covered by microbial assemblages under similar stages of development.

In the Borg El-Arab salt works, the microbial mats that flourish on the floor of the pond become somewhat buoyant due to escape of gases from decaying organic matter in the deeper subrecent sediments. The strong northwesterly wind generates a northwesterly current in the shallow marginal part of the pond, which leads to the contortion of the sticky surface of the microbial mats into ripple marks with NE–SW orientation. Also during this time, reworking of clastic gypsum and carbonate ooids from the coastal ridges move out into the pond and adhere to the sticky surface of the mats. With continued evaporation, the rising salinity of the pond leads to the death of the microbial mats and nucleation of rosette gypsum on the crinkled surface of the mats. In another season of dilution of the pond, cyanobacteria can become reestablished and flourish on the top of the gypsum layer, thus preventing further reworking by water currents. Therefore, a unidirectional ripple mark persists in the submerged part of the pond. During desiccation and exposure of this unidirectional rippled surface, the continuous escaping of organic gases from the deeper subrecent sediments leads to further deformation of the microbial gypsum layer. The polydirectional orientation of the ripple marks also may be due desiccation of the microbial mats into patches of different widths, and the preferential escape direction of the organic gases from below the microbial mats. Therefore, the surface of the ripple marks may become slightly shifted depending on the escape path of the organic gases.

In contrast, the multidirectional ripple marks in the modern lower supratidal deposits of the Mellum Island, southern North Sea are interpreted by Noffke (1998) as a result of tidal inundation in very shallow water. In the lower supratidal flat environment, reworking of the gypsum sediments by strong water currents during storms becomes dominant. The direction of the currents is frequently shifted by changing winds, which leads to the varied directions of the ripple marks. At sites of calmer hydrodynamic conditions, filamentous cyanobacteria settle on newly shaped parts and consolidate the physically generated ripple morphology by constant overgrowth.

In the Miocene gypsum of El-Barqan and Rabigh areas, the flat lying and the crinkled microbial gypsum may also develop in a similar way to that in the studied salt works and the Mellum Island, but under constant and persistent, deeper hydrodynamic conditions. In this environment, persistent water current leads to deposition of reworked gypsum with a ripple marked surface. During quiescent periods, and with a decrease in salinity and absence of burrowers and grazers, cyanobacteria flourish on the ripple marked surface and form a pavement that keeps the clastic gypsum from additional reworking during storms. These cyanobacterial mats can also entrap and bind reworked gypsum grains on their surfaces during a slight water current. Differences in the amount of entrapped gypsum crystals lead to a variable thickness of the gypsum laminae (Fig. 6a). Increases in the water energy and increase in the amount of deposition of clastic gypsum lead to burial of the cyanobacterial mat and formation of another gypsum lamina. The relatively thick (<180 cm) crinkled microbial gypsum layer indicates faster evaporation and precipitation of gypsum and a stable condition in the depositional environment in contrast to Borg El-Arab solar ponds, where the microbial gypsum layer has a thickness of less than 7 cm.

Formation of microlaminated sediments with development of cyanobacterial mats in solar ponds and Miocene gypsum occurs within a salinity range of 60–150 g/l. Cornee et al. (1992) found that cyanobacterial mats failed to colonize the less saline water (36–60 g/l) due to the action of herbivorous snails and competition for light from floating algal/bacterial masses. At higher salinity (150 g/l), gypsum begins to crystallize out of solution, and cyanobacterial mats disappear because they are incapable of growing at high salinities in excess of 150 g/l (Thomas and Geisler 1982). However, Oren et al. (1995) found different cyanobactena and purple bacteria within a gypsum crust on the bottom of a hypersaline saltern pond at salinity of 280 to 290 g 1–0 in Eilat.

The relatively exposed margin of the solar ponds is distinguished by the small size of its desiccation cracked polygons, which are known as "petee structures." These petees have no equivalence in El-Barqan or Rabigh gypsum. This is because the microbial gypsum in El-Barqan and Rabigh does not suffer from the prolonged desiccation and remains submerged most of the time. In the marginal part of the solar ponds, where the ground is moist from groundwater seepage from the pond, upward movement of water leads to a perpetually damp surface and flourishing cyanobacterial growth. Upon evaporation and increase in the salinity of the groundwater, gypsum crystals nucleate displacively below and within the cyanobacterial mats. The interplay between microbial growth, escape of biogenic gases from decayed microbial mats just below the surface, and gypsum nucleation leads to the formation of the buckled crust known as petee structures.

The transition between carbonate or siliciclastic sediments and the overlying evaporites in El-Barqan and Rabigh (respectively) is marked by assemblages of stromatolites, which display both continuous and discontinuous lamination structure. Stromatolites with continuous, uniform laminae are interpreted to have formed or are a result of in situ precipitation of pan floor-encrusting gypsum, whereas stromatolites with discontinuous lamination are formed by trapping and

binding of loose reworked gypsum in microbial mats, similar to findings and interpretation by Pope et al. (2000).

The existence of the domal stromatolite in patches in the ponds (Fig. 2d) may be similar to the formation of erosional remnants and pockets which evolve from wave and current energy that reshape the relief morphology of the mat-covered surfaces (Noffke et al. 1996; Bose and Chafetz 2009). Table-like erosional remnants are left behind after water agitation has eroded parts of the former biostabilization surface layer. These erosional remnants form sites for nucleation and growth of gypsum into domal structures.

The close similarity of the surface morphology of the domal stromatolites in El-Barqan gypsum (Fig. 7a) and Borg El-Arab salt works (Fig. 2b–d, f) does not mean that they have formed in identical environmental condition and by the same processes. In Borg El-Arab, the domal stromatolite is composed of deformed crusts over a central cavity that developed from the escape of organic gases from subrecent decayed microbial mats. On the other hand, the domal stromatolite in El-Barqan is formed of delicate microbial laminae over displacively grown gypsum crystals (Fig. 6c). Therefore, the uplift of the microbial laminae is a consequence of the displacive growth of gypsum from groundwater brine in El-Barqan, whereas the deformation of the microbial laminae at Borg El-Arab is a consequence of inflation by and later escape of organic gases below the delicate microbial layer in the dominant subaqueous environment.

In conclusion, the predominance of microbial communities in all three settings (Borg El-Arab, El-Barqan, and Rabigh) indicates a similar condition of high salinity of the brine (60–150 g/l), absence of grazers and burrowers, sufficient nutrient and oxygen supply, and low sedimentation rate and physical agitation. Minor differences in the morphology of the microbial deposits are the result of minor variations in the hydrodynamic condition of the basin and differences in the mechanisms of growth of the microbial laminae.

Acknowledgments We wish to thank Cairo University and King Abdulaziz University for the field and lab facilities offered to this work.

References

Aref MAM (1998) Holocene stromatolites and microbial laminites associated with lenticular gypsum in a marine-dominated environment, Ras El Shetan area, Gulf of Aqaba, Egypt. Sedimentology 45:245–266

Aref MAM (2000) Halite and gypsum morphologies in Borg El-Arab solar salt works-a comparison with the underlying supratidal sabkha deposits, Mediterranean Coast, Egypt. In: Proc. 5th Int. Conf. Geol. Arab World, Cairo University, Egypt, pp. 1117–1134

Aref MAM (2003) Lithofacies characteristics, depositional environment and karstification of the Late Miocene (Messinian) gypsum deposits in the Northern Western Desert, Egypt. Sedimentol Egypt 11:9–27

Aref MAM, Mandurah MH (2011) Lithostratigraphy, facies interpretation and depositional environment of the Lower Miocene gypsified stromatolites and microbial laminites, Rabigh and Ubhur areas, Red Sea Coast, Saudi Arabia. J King Abdulaziz Univ Earth Sci 22(1):117–139

Basyoni MH, Aref MAM (2007) Tepees versus petees in some Saudi and Egyptian sabkhas; factors controlling their distribution, morphology and origin. XI Congresso da Abequa, Belém, Pará, Brazil (Abstract)

Basyoni MH, Aref MAM (2011) Topographic and climatic factors controlling morphology and distribution of microbially induced sedimentary surface structures and karstic features in Rabigh coastal sabkha, Red Sea, Saudi Arabia. Arabian Conf. Geosciences, King Saud University, Riyadh (Abstract)

Beukes NJ, Lowe DY (2006) Environmental control on diverse stromatolite morphologies in the 3000 Myr Pongola Supergroup, South Africa. Sedimentology 36(3):383–397

Bose S, Chafetz HS (2009) Topographic control on distribution of modern microbially induced sedimentary structures (MISS): a case study from Texas coast. Sediment Geol 213:136–149

Cabioch G, Camoin G, Webb EG, Le Cornec F, Molina MG, Pierre C, Joachimski MM (2006) Contribution of microbialites to the development of coral reefs during the last deglacial period: case study from Vanuatu (South-West Pacific). Sediment Geol 185:297–318

Cohen RW, Castenholz R, Halvorsor HO (1984) Microbial mats: stromatolites. A. R. Liss, New York, pp 411–424

Cornee A, Dickman M, Busson G (1992) Laminated cyanobacterial mats in sediments of solar salt works; some sedimentological implications. Sedimentology 39:599–612

Costerton J, Stoodley P (2003) Microbial biofilms: protective nitches in ancient and modern geomicrobiology. In: Krumbein WE, Paterson DM, Zavarzin GA (eds) Fossil and recent biofilms. Kluwer, Dordrecht, pp 15–21

Cuadrado DG, Carmona NB, Bournod C (2011) Biostabilization of sediments by microbial mats in a temperate siliciclastic tidal flat, Bahia Blanca estuary. Sediment Geol 237:95–101

Davis JS (2009) Management of biological systems for continuously operated solar saltworks. Global Nest J 11(1):73–78

Davis JS, Giordano M (1996) Biological and physical events involved in the origin, effects, and control of organic matter in solar saltworks. Int J Salt Lake Res 4:335–347

Dill RE, Shinn EA, Jones AT, Kelly K, Steinen RP (1986) Giant subtidal stromatolites forming in normal salinity waters. Nature 324:55–58

Draganits E, Noffke N (2004) Siliciclastic stromatolites and other microbially induced sedimentary structures in an Early Devonian Barrier-Island environment (Muth Formation, NW Himalayas. J Sediment Res 74(2):191–202

Duane MJ, Al-Zamel AZ (1999) Syngenetic textural evolution of modern sabkha stromatolites (Kuwait): sediment. Geol 127:237–245

Eriksson G, Scheiber J, Bouougri E, Gerdes G, Porada H, Banerjee S, Bose K, Sarkar S (2007) Classification of structures left by microbial mats in their host sediments. In: Scheiber J, Bose K, Eriksson G, Banerjee S, Sarkar S, Altermann W, Catuneanu O (eds) Atlas of microbial mat features preserved within the clastic rock record. Elsevier B.V., Amsterdam, pp 39–52

Gerdes G (2007) Structures left by modern microbial mats in their host sediments. In: Scheiber J, Bose K, Eriksson G, Banerjee S, Sarkar S, Altermann W, Catuneanu O (eds) Atlas of microbial mat features preserved within the clastic rock record. Elsevier B.V., Amsterdam, pp 5–38

Gerdes G, Krumbein WE (1987) Biolaminated deposits. Springer, Berlin, p 183

Gerdes G, Krumbein WE, Reineck HE (1984) The depositional record of sandy, versicolored tidal flats (Mellum Island, southern North Sea. J Sediment Res 55(2):265–278

Gerdes G, Krumbein WE, Reineck HE (1991) Biolaminations—ecological versus depositional dynamics. In: Einsele G, Ricken W, Seilacher A (eds) Cycles and events in stratigraph. Springer, Berlin, pp 592–607

Gerdes G, Claes M, Dunajtschik-Piewak K, Riege H, Krumbein WE, Reineck H (1993) Contribution of microbial mats to sedimentary surface structures. Facies 29:11–13

Glunk C, Dupraz C, Braissant O, Gallagher KL, Verrecchia EP, Visscher PT (2011) Microbially mediated carbonate precipitation in a hypersaline lake, Big Pond (Eleuthera, Bahamas). Sedimentology 58(3):720–736

Jones B, Hunter IG (1991) Corals to rhodolites to microbiolites—a community replacement sequence indicative of regressive conditions. Palaios 6:54–66

Kato S, Kobayashi C, Kakegawa T, Yamagishi (2009) Microbial communities in iron-silica-rich microbial mats at deep-sea hydrothermal fields of the Southern Mariana Trough. Environ Microbiol 11 (8):2094–2111

Kendall CGSC, Skipwith P (1968) Recent algal mats of a Persian Gulf lagoon. J Sediment Petrol 38:1040–1058

Knoll AH (1985) A Paleobiological perspective on sabkhas. In: Friedman GM, Krumbein WE (eds) Hypersaline ecosystem, ecological studies 53. Springer, Berlin, pp 407–425

Krumbein WE (1983) Stromatolites. The challenge of a term in space and time. Precambrian Res 20:493–531

Krumbein WE (1985) Introduction. In: Friedman GM, Krumbein WE (eds) Hypersaline ecosystem, ecological studies 53. Springer, Berlin, pp 13–17

Logan BW, Rezak R, Ginsburg RN (1964) Classification and environmental significance of algal stromatolites. J Geology 7:68–83

Magaña GYG, Lopez JCP, Ortiz SMM, Roche ED, Davis JS (2005) Recovery of a commercial solar saltworks damaged by a hurricane: role of biological management. Proc Ninth Int Conf Environ Sci Technol A:903–912

Mandurah MH, Aref MAM (2010) Petrography and diagenesis of the Miocene secondary gypsum enriched in microbialites, Ubhur and Rabigh areas, Red Sea coast, Saudi Arabia. Sedimentol Egypt 18:73–88

Mandurah MH, Aref MAM (2011) Lithostratigraphy and standard microfacies types of the Neogene carbonates of Rabigh and Ubhur areas, Red Sea coastal plain of Saudi Arabia. Arab J Geosci. doi:10.1007/s12517-011-0281-z

Moore TA, Al-Rehaili MHA (1989) Geologic map of the Makkah quadrangle, sheet 21D. Kingdom of Saudi Arabia. Ministry of Petroleum and Mineral Resources, Jeddah

Noffke N (1998) Multidirected ripple marks rising from biological and sedimentological processes in modern lower supratidal deposits (Mellum Island, southern North Sea. Geology 26:879–882

Noffke N, Gerdes G, Klenke T, Krumbein WE (1996) Microbially induced sedimentary structures—examples from modern sediments of siliciclastic tidal flats. Zbl Geol Paläontol I:307–316

Noffke N, Gerdes G, Klenke T, Krumbein WE (2001) Microbially induced sedimentary structures—a new category within the classification of primary sedimentary structures. J Sediment Res 71:649–656

Noffke N, Gerdes G, Klenke T, Krumbein WE (2007) Microbially induced sedimentary structures indicating climatological, hydrological and depositional conditions within recent and Pleistocene coastal facies zones (Southern Tunisia). Facies 44(1):23–30

Oren A, Kuhl M, Karsten U (1995) An endoevaporitic microbial mat within a gypsum crust: zonation of phototrophs, photopigments, and light penetration. Mar Ecol Prog Ser 128:151–159

Oren A, Sørensen KB, Canfield DE, Teske AP, Ionescu D, Lipski A, Altendorf K (2009) Microbial communities and processes within a hypersaline gypsum crust in a saltern evaporation pond, Eilat, Israel. Hydrobiologia 626(1):15–26

Orti Cabo F, Pueyo-Mur JJ, Geisler-Cussey D, Dulau N (1986) Evaporitic sedimentation in the coastal salinas of Santa Pola (Alicante, Spain). Rev Invest Geol 38(39):169–220

Pope MC, Grotzinger JP, Schreiber BC (2000) Evaporitic subtidal stromatolites produced by in situ precipitation: textures, facies association and temporal significance. J Sediment Res 70:1139–1151

Russell M, Grimalt JA, Hartgers WA, Taberner C, Rouchy JM (1997) Bacterial and algal markers in sedimentary organic matter deposited under natural sulphurization conditions (Lorca Basin, Murcia, Spain). Org Geochem 26:605–625

Scheiber J (2004) Microbial mats in the siliciclastics record—a summary of the diagnostic features. In: Eriksson G, Altermann W, Nelson DR, Mueller WU, Catuneanu O (eds) The precambrian earth: tempos and events. Developments in Precambrian geology 12. Elsevier, Amsterdam, pp 663–673

Scheiber J, Bose K, Eriksson G, Banerjee S, Sarkar S, Altermann W, Catuneanu O (eds) (2007) Prologue: an introduction to microbial mats. In: Atlas of microbial mat features preserved within the clastic rock record. Elsevier B.V., Amsterdam, pp. 1–4

Schreiber BC, Philip RP, Benali S, Helman ML, de la Pena JA, Marfil R, Landais A, Cohen AD, Kendall CGSC (2001) Characterization of organic matter formed in hypersaline carbonate/evaporite environments: hydrocarbon potential and biomarkers obtained through artificial maturation studies. J Petrol Geol 24:309–338

Semikhatov MA, Gebelin CD, Cloud P, Benmore WC (1979) Stromatolite morphogenesis: progress and problems. Canad J Earth Sci 16:992–1014

Stivaletta N, Barbieri R, Bosco M, Picard C, Ori GG, Marinangeli L (2006) Microbial communities from continental sabkhas of southern Tunisia: terrestrial analogues of mars evaporite environments. Lunar and Planetary Science 37 poster abstract 1608.

Taher AG, Abd El Wahab S, Philip G, Krumbein WE, Wali AM (1995) Evaporitic sedimentation and microbial mats in a salina system (Port Fouad, Egypt). Int J Salt Lake Res 4:95–116

Taj R (2012) Lower Miocene coastal lagoon carbonates and evaporites of Rabigh Area, Red Sea Coast, Saudi Arabia. J King Abdulaziz Univ Mari Sci (in press).

Taj RJ, Aref MAM (2009) Sediment characteristics and petrography of marginal marine ephemeral saline pans, Shuaiba Lagoons, Red Sea coast, Saudi Arabia. Sedimentol Egypt 17:27–44

Taj RJ, Aref MAM (2011) Recent sediments volcanoes and mounds induced by microbial activity in a coastal sabkha setting between Jeddah-Shuaiba areas, Red Sea, Saudi Arabia. Arabian Conference on Geosciences, King Saud University, Riyadh (Abstract)

Taj RJ, Hegab OAR (2005) Dafin formation—lithostratigraphy, sedimentology, depositional environments, Rabigh area, Saudi Arabia. Internal Report, KAU. Project No. 202/423. King Abdulaziz University, Jeddah, Saudi Arabia, p. 172

Thomas J, Geisler D (1982) Peuplements benthiques a Cyanophycees des salins de Mediterranee occidentale. Int Cong Sedimentol 11:171pp

Warren JK (1982) The hydrological significance of Holocene tepees, stromatolites and boxwork limestones in coastal salinas in South Australia. J Sediment Petrol 52:1171–1201

Webb GE, Baker JC, Jell JS (1998) Inferred syngenetic textural evolution in Holocene cryptic reefal microbialites, Heron Reef, Great Barrier Reef, Australia. Geology 26:355–358